

# Influence of an extensive green roof in the non-linear structural behavior of self – construction households

## Influencia de un techo verde extensivo en el comportamiento estructural no lineal de viviendas de autoconstrucción

O. Contreras <sup>1\*</sup>, F. Nuñez \*

\* Pontificia Universidad Javeriana – Bogota D.C, COLOMBIA

Fecha de Recepción: 09/04/2021  
Fecha de Aceptación: 22/07/2021  
PAG 157-172

### Abstract

*In recent years, ideas such as green roofs gained importance as an alternative for environmental adaptation of society to new ambient conditions. In Bogotá city, the roofs at popular neighborhood represent a potential area for their implementation. This present research discusses how the weight of a green roof impacts a self-construction dwelling unit from a structural capacity demand point of view. Green roof weight is a random variable whose normality was investigated through the Shapiro-Wilk goodness of fit. The magnification factors for this dead-like load come from the Nowak-Collins method using the confidence intervals on the mean weight value. The ATC-40 pushover methodology helped in finding the non-linear behavior of a controlled but similar structure as those found in the popular neighborhoods of Bogotá city. According to this methodology, damage caused on these structures due to seismic demand increases by the green roof incorporation. However, damage increase is a function of local soil conditions.*

**Keywords:** Green roof, probabilistic analysis, Opensees, Pushover, self-construction households

### Resumen

En años recientes, ideas como los techos verdes han ganado importancia como alternativa de adaptación ambiental de la sociedad a las nuevas condiciones del entorno. En la ciudad de Bogotá, los techos en barrio populares representan un área potencial para su implementación. La presente investigación discute el impacto del peso de un techo verde en una unidad de vivienda de autoconstrucción desde el punto de vista de la demanda de capacidad estructural. El peso del techo verde es una variable aleatoria cuya normalidad se investigó mediante la prueba de bondad de ajuste de Shapiro-Wilk. Los factores de magnificación para esta carga muerta provienen del método de Nowak-Collins usando intervalos de confianza sobre el valor medio del peso. A través de la metodología "Pushover" propuesta en el ATC-40 se encontró el comportamiento no lineal de una estructura de control similar a las que se encuentran en los barrios populares de la ciudad de Bogotá. De acuerdo con esta metodología, el daño causado en estas estructuras debido a la demanda sísmica aumenta por la incorporación del techo verde. Sin embargo, el incremento de los daños depende de las condiciones locales del suelo.

**Palabras clave:** Análisis probabilista, Opensees, Pushover, techo verde, viviendas de autoconstrucción

## 1. Introduction

*Over the last few decades, the effects of climate change and environmental degradation left consequences throughout the world. Environmentally sustainable ideas represent a way to mitigate the effects. From an environmental point of view, green roofs are defined as a tool that reduces the thermal sensation in urban areas while retaining runoff by alleviating the flow of rainwater in the sewer system, by improving air quality (Aboelata, 2021).*

*From a structural perspective on one hand, green roofs can be defined as just one added load on the roof of a house. On the other hand, this load tends to be variable depending on the climate conditions of the area, due to changes in weight of the substrate of plants as saturation can happen. With the increase in the mass of the last story of a house, the potential inertial force of this story also increases as a result of an external force for example seismic forces. As consequence, the horizontal displacement of the structure also increases. Thus, increasing the upper story mass in a structure, increases the probability of developing a new failure mechanism. For the present research a Self-Construction-Households (SCH) define an unregulated popular masonry dwelling unit, that in most cases lacks structural design. However, these SCH constitute also a large area in the city for green roof potential implementation. In the municipality of Soacha there was a productive green roof alternative using plastic bottles containers in a house built with modular concrete panels embedded in thin sheet profiles made of galvanized steel.*

---

#### Corresponding author:

Pontificia Universidad Javeriana– Bogota D.C, COLOMBIA  
E-mail: contreras.o@javeriana.edu.co



The roof of this house got four uniaxial seismic accelerometers and through computational modeling, the researchers reported an increase of 241% in the tensile stresses associated with the load combinations and a 56% increase in natural structural period (Olaya et al., 2014). A study using numerical methods characterized a reinforced concrete moment resistance frame, with a 3, 6 and 8 story configurations. This structure was designed in accordance with current regulatory standards without accounting the weight of green roof. Structural natural periods increased 5.75%, 3.03% and 2.29% for the 3, 6 and 8 story frames respectively, compared to a normal gravel roof finish (Bianchini et al., 2016). Within a life cycle investigation for green buildings carried out in 2017, non – linear plus fragility analysis helped in analyzing a 4-story-high commercial building designed in reinforced concrete. Intensive and extensive green roof models experienced a slightly earlier loss of lateral load capacity at a roof drift ratio of around 4% due to significant P-Delta effects. This is evidence of an increase in the structural period of 5.34% and 8.15% respectively with respect to the structure without green roof (Welsh-Huggins & Liel, 2017).

Current knowledge of the influence of a green roof from a structural point of view focuses on properly design of reinforced concrete and precast concrete structures. The present research studies the non-linear behavior of typical SCH in Bogotá based on moment-resistant concrete frames neither with structural design nor confined masonry under the presence of a green roof.

## 2. Green roofs

Green roofs are a sustainable means that help to mitigate negative effects on the environment. Amongst the main advantages they represent there are tax benefits for the owner of said green roof, better air quality, rainwater retention and an increase in the commercial value of the property (Manso et al., 2021). (Figure 1) shows an alternative construction option. This demonstrates the community's interest in this sustainable mechanism and allows the development of research that contributes to the analysis of both environmental benefits and structural effects.



**Figure 1.** Alternative green roof (Apuntes, 2020)

Green roofs are globally classified as extensive (thickness<15cm) or intensive (thickness>15cm) (Nektarios et al., 2021). These are generally made of a waterproofing layer to avoid contact between the support structure and biological elements, a drainage layer which allows the passage of water but not solid elements, a filtration layer where the substrate is contained, a layer of substrate and finally the vegetation layer. The growth medium is made up of materials that increase in weight when a humid condition is present. In such a way green roof mass depends directly on the climate characteristics of the area where it is, the type of plants in the vegetal layer, the retention capacity of the roof in its different layers and the evaporation rate (A'saf et al., 2020).

## 3. Green roof weight

Typical green roof in Bogotá city include slag, rice husk, compost, coconut chip, pine chip, organic soil, and river sand. In saturated condition, densities range from 760 kg/m<sup>3</sup> to 2190 kg/m<sup>3</sup> (Cascone et al., 2018). A Shapiro Wilk test performed on samples of 21 examples of green roofs, considering significance levels of 0.1, 0.05,

0.02 and 0.01, let to a Normal probability distribution function. Using different thicknesses for substrate is a common practice allowing different vegetal species during a green roof solution design. Having the information of 11 projects, helped in characterizing these green roof solutions accounting local solutions based on the catalog of vegetation in domestic gardens in Bogotá (Sierra Guerrero and Amarillo Suárez, 2014) and the Bogotá green roof guide. Subsequently, the probable thickness that each type of plant should have to survive local weather conditions is a function of natural conditions. A satellite image analysis helped in determining the approximate area covered in green roofs. A safety factor calibration methodology helped to find the average weight approximately at 208.05 kg/m<sup>2</sup>. The following steps show the methodology followed to determine said factors.

- Step-1. Formulate the limit state function and the design equation.
- Step-2. Obtain the initial design point for the number of random variables ( $n - 1$ ) name it  $X_i^*$ .
- Step-3. Compute the normal equivalent for the non-normal probability distribution functions of the random variables ( $\mu_{X_i}^e$ ), ( $\sigma_{X_i}^e$ ).
- Step-4. Determine the partial derivatives of the limit state function.
- Step-5. Calculate the column vector  $\alpha$  using (Equation 1):
- 

$$[\alpha] = \frac{[\rho]G}{\sqrt{G^t[\rho]G}} \quad (1)$$

- Step-6. Determine the new design point in reduced variants (Equation 2).

$$Z_i^* = \alpha_i \beta_{target} \quad (2)$$

Where  $\beta_{target}$  is the reliability of the target to be found.

- Step-7. Determine the value of the corresponding design point in original coordinates (Equation 3).

$$X_o^* = \mu_{X_i}^e + Z_i^* \sigma_{X_i}^e \quad (3)$$

- Step-8. Determine the value of the remaining random variable (Equation 4).

$$\mu_{X_i} = \frac{X_i^*}{1 + \alpha_i \beta V_{X_i}} \quad (4)$$

Where  $V_{X_i}$  is the coefficient of variation of the random variable

- Step-9. Repeat steps 3 through 8 until  $\alpha$  converges
- Step-10. Once it converges, the design factor comes from (Equation 5):

$$\gamma_i = \frac{X_i^*}{\bar{X}_i} \quad (5)$$

For step 1 the limit state function is a linear function as follows (Equation 6):

$$g(\mathbf{R}, \mathbf{L}, \mathbf{D}) = \mathbf{R} - \mathbf{L} - \mathbf{D} \quad (6)$$



Where  $R$  is the resistance,  $D$  is the green roof dead load and  $L$  is the live load. The design equation is (Equation 7):

$$\phi R_n \geq \gamma_D D_n + \gamma_L L_n \quad (7)$$

Where  $\phi$ ,  $\gamma_D$  and  $\gamma_L$  are safety factors for resistance, dead load and live load respectively. In step 2, the design points correspond to the mean value of the random variables (identified with an asterisk as a superscript). For live load, a Gumbel type I probability distribution function is used (Arroyo Amell and Ramos Castillo, 2015), and for structural resistance a LogNormal distribution (Nowak and Collins, 1976). A ratio between live load and twice the dead load is used as suggested by Nowak and Collins, and from the following equations (Equation 8):

$$g(R, L, D) = \mu_R - \mu_L - \mu_D = 0 \quad (8)$$

The design point of the resistance is, then (Equation 9):

$$r^* = 3\mu_D \quad (9)$$

In step 3, the equivalent for resistance as a normal probability function has the following parameters (Equation 10) and (Equation 11):

$$\mu_R^e = r^* [1 - \ln r^* + \ln \mu_R] \quad (10)$$

$$\sigma_R^e = r^* V_R \quad (11)$$

where  $V_R$  is the coefficient of variation for resistance, which for reinforced concrete elements is considered as 0.12 (Arroyo Amell and Ramos Castillo, 2015). The normal equivalent for the probability function of the live load uses the following parameters (Equation 12) (Equation 13) and (Equation 14):

$$\sigma_L^e = \frac{1}{f_L(l^*)} \phi[\Phi^{-1}(F_L(l^*))] \quad (12)$$

$$F_L(l^*) = \exp[-\exp(-a(l^* - u))] \quad (13)$$

$$a = \sqrt{\frac{\pi^2}{6\sigma_L^2}} = \frac{\pi}{\sqrt{6}(V_L \mu_L)} \quad (14)$$

where  $V_L$  is the coefficient of variation of the live load, which is considered as 0.25 (Galambos et al., 1982) (Equation 15) (Equation 16):

$$u = \mu_L - \frac{0.5772}{a} \quad (15)$$

$$f_L(l^*) = a[\exp(-a(l^* - u))]F_L(l^*) \quad (16)$$



The partial derivatives obtained from step 4 are (Equation 17):

$$G_1 = -\frac{\partial g}{\partial R} \sigma_R^e = -\sigma_R^e \quad (17)$$

(Equation 18)

$$G_2 = -\frac{\partial g}{\partial D} \sigma_D = \sigma_D = V_D \mu_D \quad (18)$$

(Equation 19)

$$G_3 = -\frac{\partial g}{\partial L} \sigma_L^e = \sigma_L^e \quad (19)$$

Where  $V_D$  is the coefficient of variation of dead load, which according to results previously obtained corresponds to 0.23. For step 5 the matrix  $\alpha$  indicates the relationship between the random variables under consideration. Each variable is considered to be independent (Nowak and Collins, 1976). In step 6 for the calculation of the new design point in reduced variants,  $\beta$  values are 0.5, 1.0, 1.5, 2.0, 2.5, 3.0, 3.5, and 4.0 since a single  $\beta$  value is not related to this type of structures. The reduced variants are (Equation 20) (Equation 21):

$$Z_D^* = \alpha_D \beta \quad (20)$$

$$Z_L^* = \alpha_L \beta \quad (21)$$

The design points in the original coordinates (see step 7) are (Equation 22):

$$d^* = \mu_D + Z_D^* \sigma_D = \mu_D (1 + Z_D^* V_D) \quad (22)$$

(Equation 23)

$$l^* = \mu_L^e + Z_L^* \sigma_L^e \quad (23)$$

(Equation 24)

$$r^* = d^* + l^* \quad (24)$$

In step 8 the average value for the resistance is (Equation 25):

$$\mu_R = \frac{r^*}{1 + \alpha_R \beta V_R} \quad (25)$$

Convergence rapidly reports a safety factor for green roof weight of 1.1, according to (Equation 26):

$$\gamma_D = \lambda_D \frac{d^*}{\mu_D} \quad (26)$$

So, then for weight, a normal distribution function works with a mean value of 228.86 kg/m<sup>2</sup> and a standard deviation of 52.65 kg/m<sup>2</sup> as shown in (Figure 2).



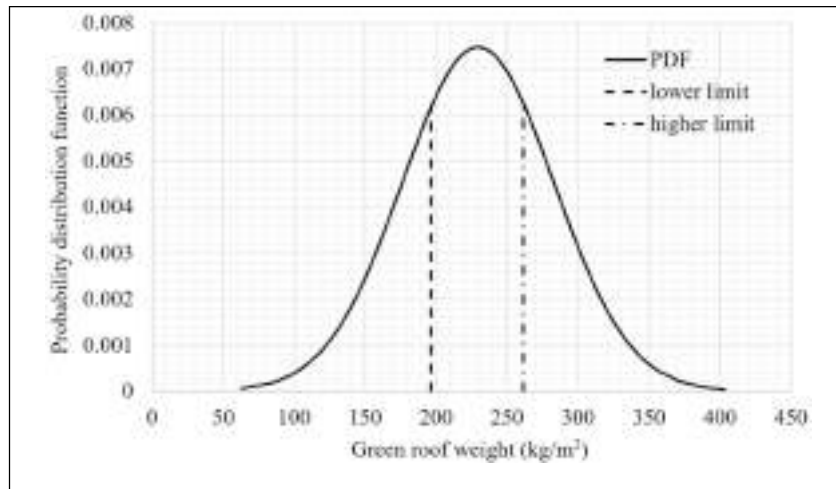


Figure 2. Probability function of a green roof weight

A confidence interval on the mean value for a green roof seems a better tool for all probability purposes. Thus, the following equations (Equation 27) and (Equation 28) state the limits:

$$\text{Lower limit: } \mu - \frac{Z_{\alpha/2}}{\sqrt{n-1}} \quad (27)$$

$$\text{Higher limit: } \mu + \frac{Z_{\alpha/2}}{\sqrt{n-1}} \quad (28)$$

where  $\alpha = 0.05$  to consider a 95% probability of certainty  $1 - 0.05 = 0.95$  and  $Z_{\alpha/2}$  corresponds to the value of the area under the normal distribution curve at a point  $\frac{\alpha}{2}$  (Montgomery and Runger, 2010).

#### 4. Self-Construction Households (SCH)

Urban planning failures from the conception of Bogotá city, led to an unplanned, disorganized and unqualified construction activity know as SCH, which currently populate vast areas of the city. Due to budget constraints, a formal construction is not a solution for a large portion of Bogotá's population. Thus, SCH are a solution to shelter families within the city. This phenomenon started to grow as early as the 1960s (López Borbón, 2018). Even though SCH have basic services such as water and electricity, they lack structural design, representing a liability for owners. Ancient construction knowledge is part of Colombia architectural heritage. However, it doesn't account the need for a rigorous study and seismic capacity, which nowadays, is mandatory. In the following part of this document, there is a brief description of a typical SCH in terms of geometry, materials and their constitutive models used to perform non-linear analysis.

#### 5. SCH scope geometries

A total of three SCH models of 1, 2 and 3 stories helped to understand the structural response when a green roof is present, after construction. The distribution of spaces is such that 35% of the length of the walls are in a transverse direction and 65% in a longitudinal direction. (Figure 3) depicts the floor plants for each one of the stories for a typical SCH.

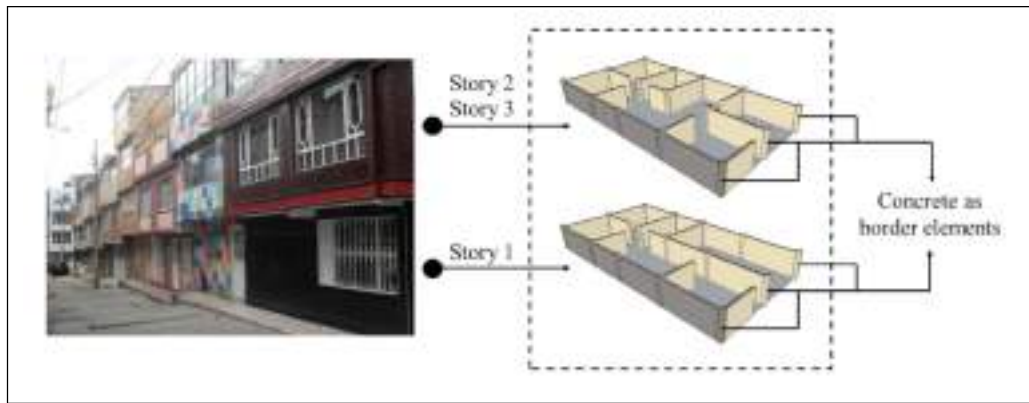


Figure 3. SCH dwelling unit (López, 2016)

The typical SCH structural system consists of clay masonry, confined by square concrete elements, reinforced with four N°4 bars as main longitudinal reinforcement, and N°3 stirrups spaced every 0.25m, with a concrete cover of 4cm. Gravity loads act on the model's nodes. Dead load come from volume and specific weight of both concrete and masonry elements. Live load bases its magnitude on the seismic resistant construction regulations of Colombia. A reduction of 25% on live load helps in computing non-linear behavior while adding a dead load at the same time. Green roof loading took place in the highest story only.

## 6. Materials

Structural analysis used OpenSees including three main materials for structural definition: concrete, masonry and steel. The degree of concrete confinement is a function of transverse reinforcement separation. According to the model proposed by (Mander et al., 1989), with a separation of 0.2m between stirrups, the effective confinement stress is zero. The constitutive model for concrete follows the parameters described in (Mohd Yassin, 1994)(Table 1) (Figure 4).

Table 1. Parameters of concrete constitutive material

Parameter	Value
$f_{pc}$ (kPa)	21000
$eps_{c0}$	0.002
$f_{pcu}$ (kPa)	12089.79
$eps_{cU}$	0.00495
$\lambda$	0.1743
$f_t$ (kPa)	2841.197
$E_{ts}$ (kPa)	3660300

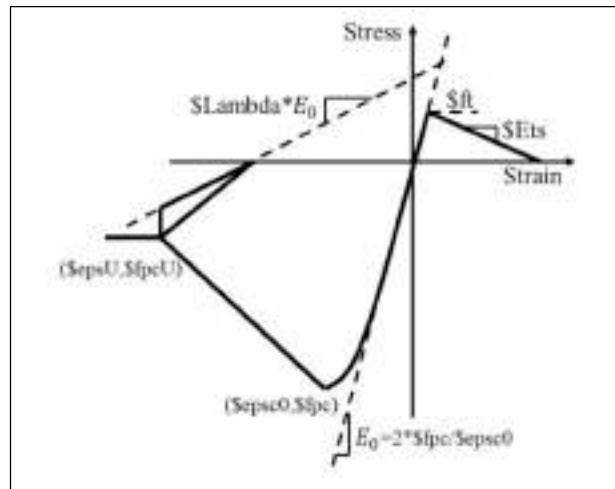


Figure 4. Constitutive model for concrete (Mohd Yassin, 1994)

Where  $f_{pc}$  is the compressive strength of the concrete,  $\epsilon_{psc0}$  is its maximum strain at  $f_{pc}$ ,  $f_{pcu}$  is the ultimate resistance of the concrete,  $\epsilon_{psu}$  is the crushing strain,  $\lambda$  is the relationship between the unloading from compression slope in  $\epsilon_{psu}$  and the initial slope,  $f_t$  is the tensile strength and  $E_{ts}$  is the tensile modulus of elasticity. A fiber model with plastic distribution using five integration points helped in accounting the  $P - \Delta$  transformation for compression members.

For steel hysteresis, the constitutive model presented in (Scott and Filippou, 2016) was part of the present analysis, with the following parameters: (Table 2) (Figure 5)

Table 2. Parameters for steel constitutive material

Parameter	Value
$e1p$ (kPa)	444000
$s1p$	0.002
$e2p$ (kPa)	674000
$s2p$	0.13
$e3p$ (kPa)	134800
$s3p$	0.15

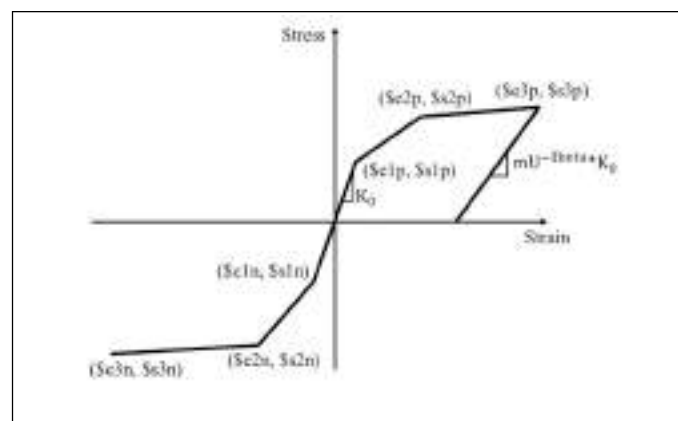


Figure 5. Constitutive model for steel (Scott & Filippou, 2016)



Where  $e_{1p}$  is the yield stress in tension,  $s_{1p}$  is the yielding strain,  $e_{2p}$  is the ultimate tensile strength (UTS),  $s_{2p}$  is the strain at the UTS,  $e_{3p}$  is considered as 20% of the last stress in tension and  $s_{3p}$  is the corresponding strain. The same magnitudes are considered in the compressive direction of stresses and strains due to the isotropic properties of steel. Confined masonry is widely used in Latin America, however neither structural analysis nor safety controls are mandatory for its design, mainly due to limited local resources and the lack of an effective management and control policy in the construction sector. The diffusion of this type of structures towards a more efficient application requires a better understanding of their structural behavior (Marques et al., 2020). In order to model the impact of masonry on the structure, the equivalent diagonal strut model is used. Figure 6 presents this model, which consists of a diagonal element whose width depends on the relative flexural stiffness of the masonry with respect to the columns of the surrounding frame (Al-Chaar and Lamb, 2002). Said element is modeled to receive only axial forces and since it is considered a constitutive model of zero tensile strength, in the pushover analysis only one of the two elements contribute to the stiffness of the structure.

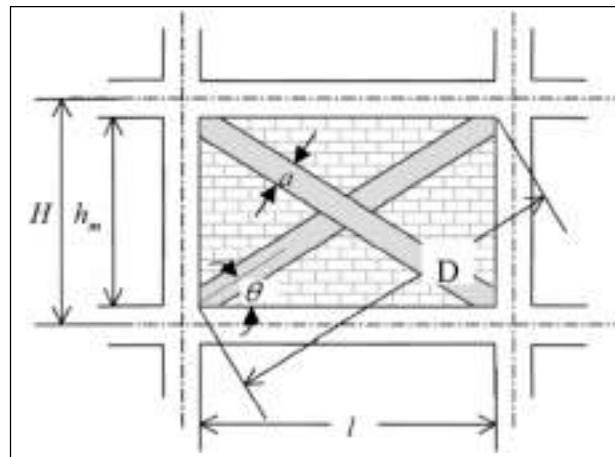


Figure 6. Equivalent diagonal strut model (Al-Chaar & Lamb, 2002)

A set of two typical masonry units available locally helped in modeling the compressive response of such composite element. The ANSYS model is available in (Figure 7).

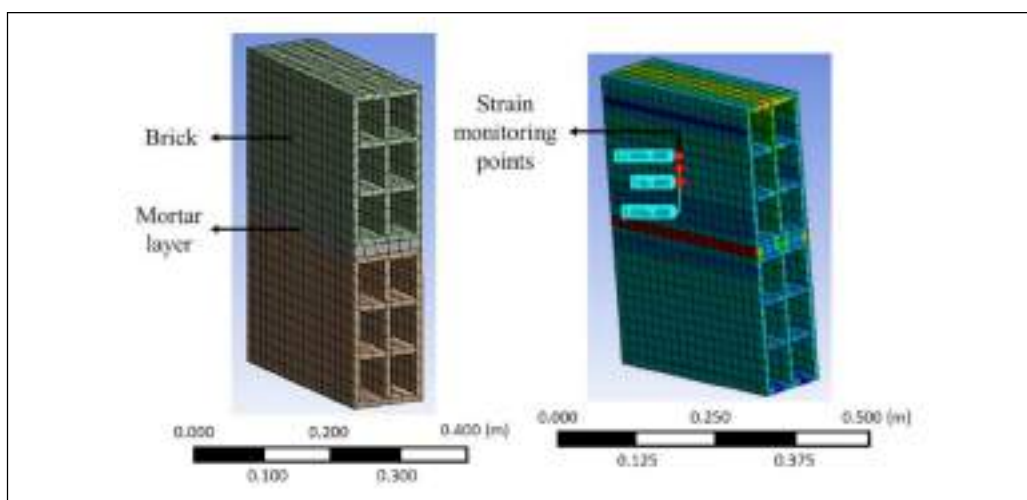
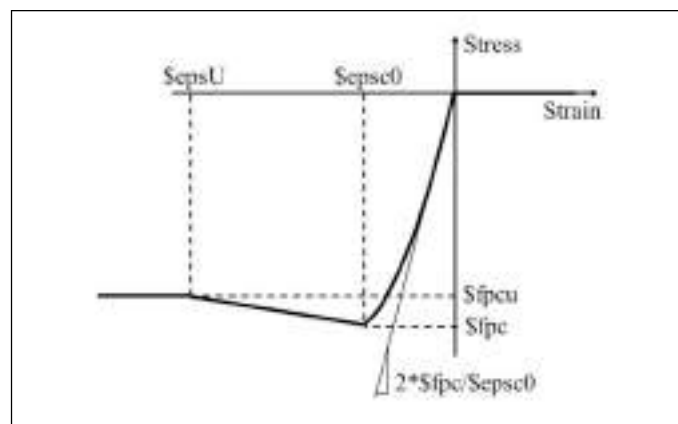


Figure 7. Finite element model of masonry

In this model, the assumed compressive strength for mortar  $f'_{m0}$  was of 7.5 MPa (Valbuena Porras & Mena Serna, 2011) having a thickness of 17mm. This value varies from 13 mm (Rincon, 2010) to 20 mm (Fundación Suiza de Cooperación para el Desarrollo Técnico, 2016). Since this thickness is variable and depends on the builder's skills, a mean value of 17 mm is chosen with a lime-to-sand ratio of 1:4 commonly used for simple masonry (Sánchez de Guzmán, 2001). The Kent-Scott-Park model (Filippou and Mazzoni, 2014) for masonry helped in setting the parameters as masonry constitutive model. These parameters are available in (Table 3) (Figure 8).

**Table 3.** Parameters of masonry constitutive material

Parameter	Value
$f_{pc}$ (kPa)	6250
$eps_{c0}$	0.00431
$f_{pcU}$ (kPa)	6250
$eps_{cU}$	0.005



**Figure 8.** Kent-Scott-Park constitutive model for masonry units (Filippou and Mazzoni, 2014)

Where  $f_{pc}$  is the masonry compressive strength,  $eps_{c0}$  is the maximum associated strain,  $f_{pcU}$  is the crushing strength of the material and  $eps_{cU}$  is the strain at the crushing strength.

## 7. Load pattern applied for the non-linear analysis

The application of the Pushover methodology involves the gradual pushing of the structure in one direction to observe its behavior as it goes into the non-linear range. However, the applied monotonic load pattern can follow several options. There are reports of lateral loads following an increasing triangular or uniform shape along the structure's height (Abhilash et al., 2009). However, inertial loading patterns arise with a debate about its applicability to seismic demands (Rahmani et al., 2019). In order to consider this effect, a lateral load pattern could be proportional to the main mode of vibration of the structure (R & S, 2000). This means neglecting the contribution of the other modes of vibration. For this research, the triangular load pattern was appropriate, since it provides an excellent approximation of the seismic capacity curve for medium and low rise structures (Sun et al., 2003). At the same time even though the load distribution is not accurate, the errors are on the security side as it underestimates the structural capacity (Khoshnoudian et al., 2011). The triangular shape, and the load distribution is available in (Figure 9):



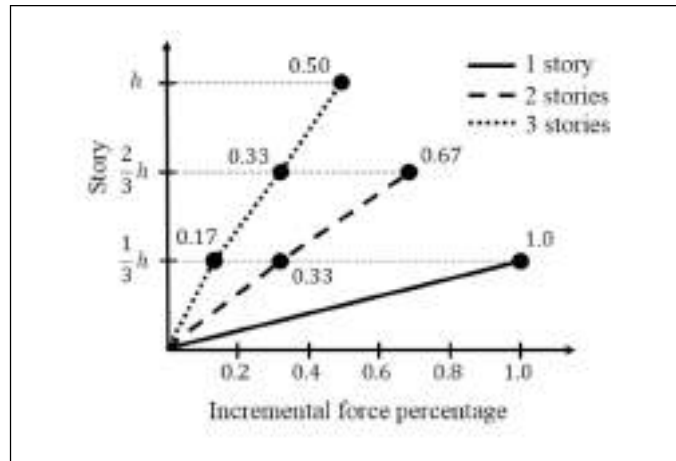


Figure 9. Lateral loading pattern

## 8. Demand and capacity curves

To calculate the performance of a buildings with a specific target displacement or until the structure reaches a collapse limit which allows to show the weaknesses of the original design (Bhandari, 2020). In other words, this analysis finds a correlation between applied lateral load and roof sway. The structure is subjected to gravity loads and static lateral loads that increase monotonically. (Figure 10) presents the results obtained from said analysis applied to the scope SCH. In all cases there is evidence of a decrease in the capacity of the structure with the presence of an extensive green roof. It is interesting to see that the smaller the mass of the structure, the higher the force-to-base shear ratio.

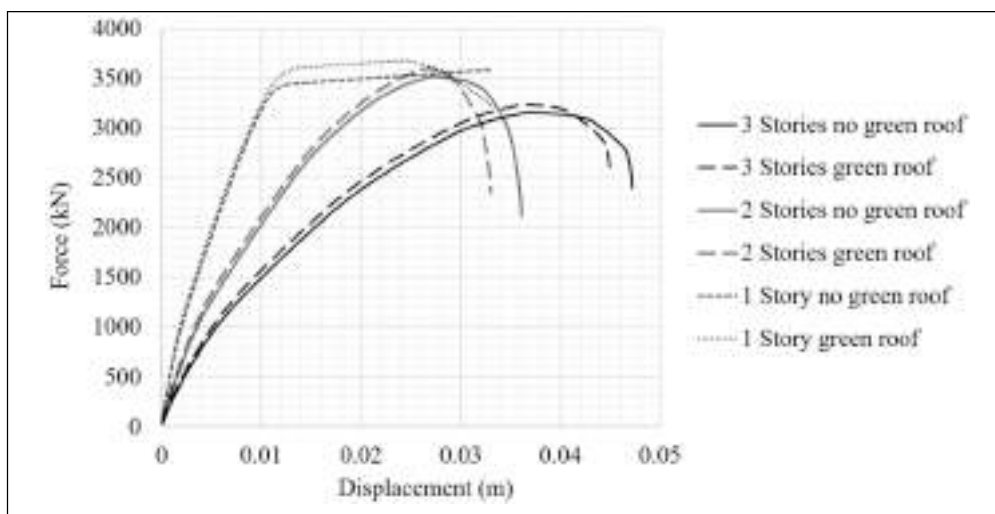


Figure 10. Capacity curve of the self-construction-households

The seismic demand in Bogotá uses on the seismic microzoning of the city. (Figure 11) shows the distribution of the 16 seismic response classifications available as a function of soil type.



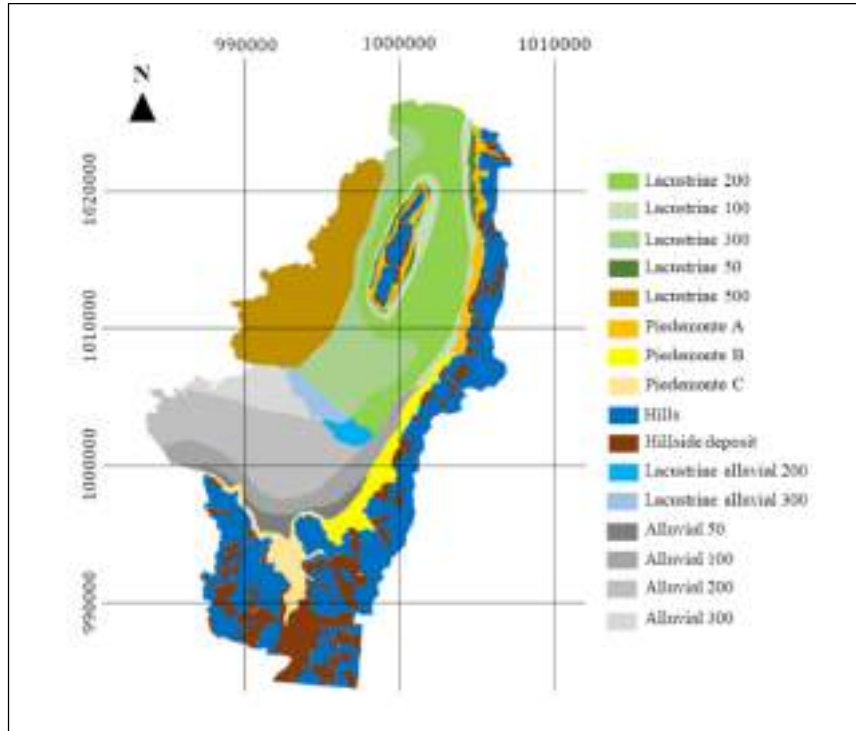


Figure 11. Seismic microzoning of Bogotá (IDIGER, 2020)

For the capacity curves and for the reduced demand curves, it was useful to use the transformation to the standard format, by means at the Acceleration Displacement Response Spectrum (ADRS). Said graphs use the spectral pseudo acceleration  $S_a$  and the spectral pseudo displacement ( $S_d$ ). For the capacity curve, (Equation 29) (Equation 30) then:

$$S_a = \frac{V_b/W}{M_k \cdot g} \quad (29)$$

$$S_d = \frac{\Delta_{roof}}{P_k \cdot \phi_{k,roof}} \quad (30)$$

Where  $V_b$  is the shear at the base,  $W$  is the weight of the structure,  $M_k$  is the mass participation factor,  $g$  is the magnitude for earth's gravity acceleration, ( $9.81 \text{ m/s}^2$ ),  $\Delta_{roof}$  is the displacement at the control node,  $P_k$  is the modal participation factor. And  $\phi_{k,roof}$  is the modal amplitude with respect to the  $k$ -th vibration mode. The subscript  $k$  indicates the vibration mode corresponding to the analysis. (Equation 31) For the demand curve:

$$S_d = \frac{T^2}{4\pi^2} S_a \quad (31)$$

Where  $T$  is the period of the structure in seconds.

## 9. Performance point

The performance point is known as the intersection between the capacity curve and the demand curve in ADRS coordinates. (Figure 12) shows the intersection of the capacity curve with the demand curve, taking place in early values of  $S_a$ . According to the displacement-based design approach, it is necessary to define seismic performance levels, which are associated with a level of damage exhibited by structures that are commonly identified through deformations or drift limits (Aşıkoğlu et al., 2020). For this study, the performance levels base their criteria on experimental investigation performed in Peru where a house made of perforated bricks, studied the effects of horizontal forces acting on the structure. As a result, the following ranges of levels of performance are available: at 13% of the curve measured horizontally corresponds to an immediate occupancy (IO) level where the damage is minor, at 32% the performance level is life safety (LS) with moderate damage, and finally with a 39% collapse prevention (CP) is the corresponding level (Zavala Toledo, 2019).

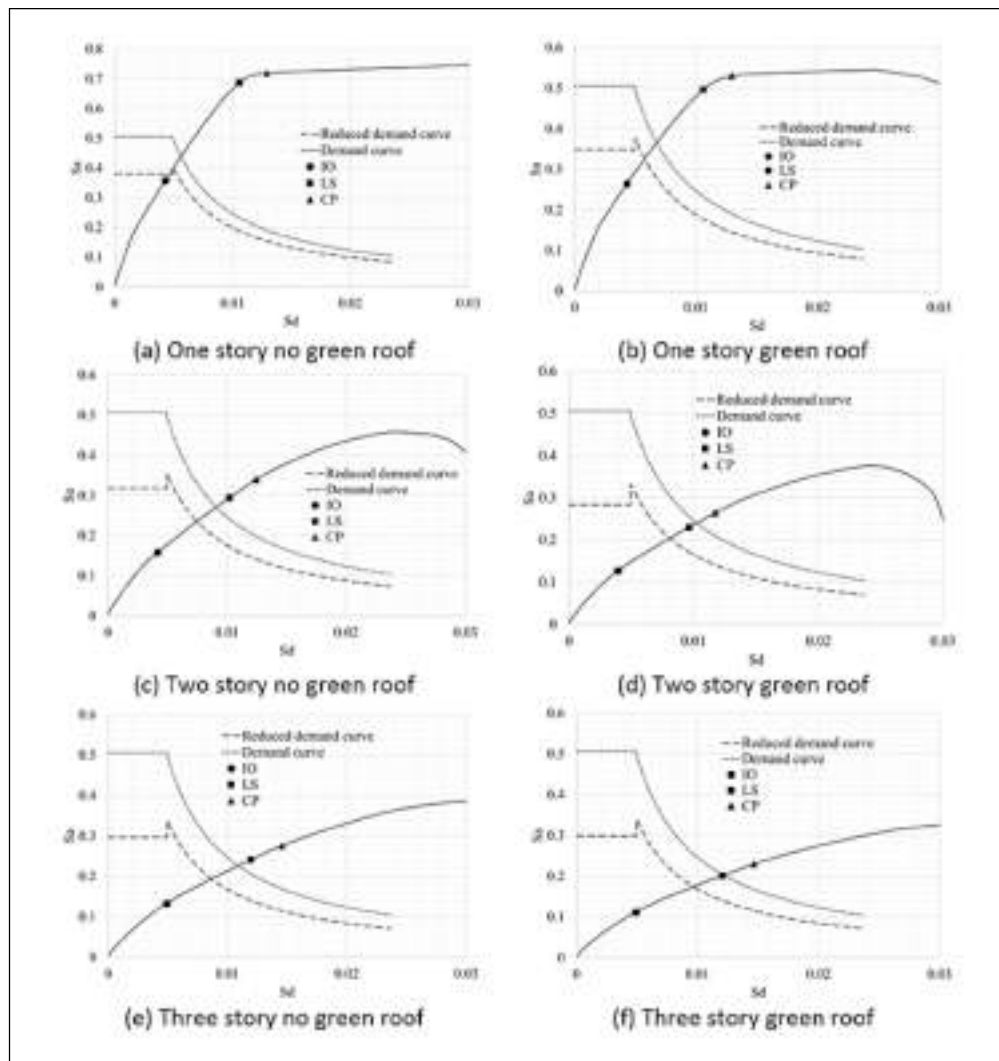
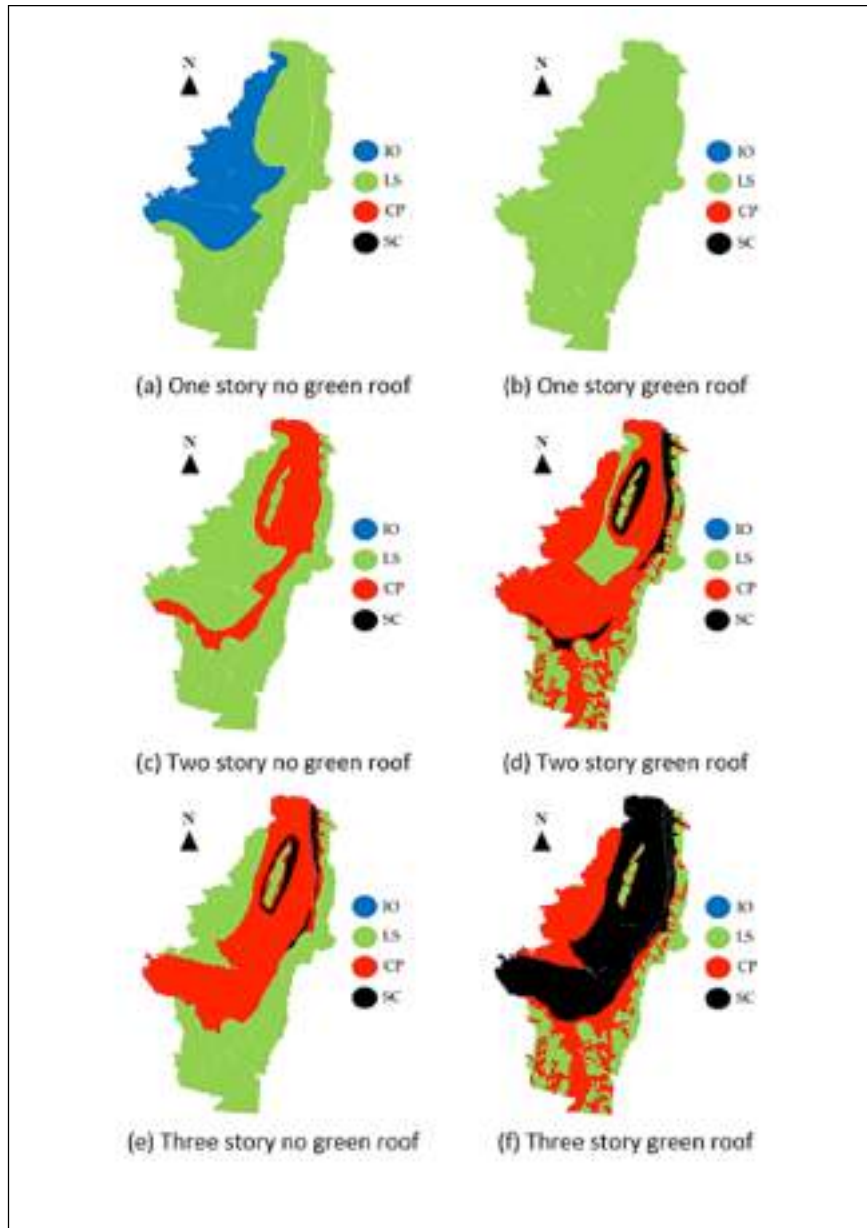


Figure 12. Pushover curves for the SCH structures located at hills soil



ENGLISH VERSION.....

The performance limits are plotted on the capacity curve in order to show the level at which the performance point happens. For example, for a two-story house without a green roof, placed at the “Hills” soil type, the performance is at the life safety level (LS). This procedure repeated the procedure to study the 1, 2 and 3-story house models in each of the 16 types of soil condition. (Figure 13) shows the performance status for the analyzed models considering the action of the green roof load.



**Figure 13.** Performance of SCH with and without the presence of a green roof in several localities of Bogotá

It is evident that the use of a green roof on these structures can cause in certain areas of the Bogotá a noticeable increase in the performance level expected from the structure in terms of seismic activity. The hills soil type seems to be the only one that does demand lower forces at the SCH, remaining the performance level in (LS).

ENGLISH VERSION.....

(Welsh-Huggins and Liel, 2017) presents an increase in the capacity curve for a reference reinforced concrete structure. This, due to the use of a shallow and a deep green roof. The results obtained in the present research are similar even though the present study is made of concrete and masonry. In contrast, in the work done by (Olaya et al., 2014) and (Bianchini et al., 2016) there is an increase in floor drift. It is not feasible to make a numerical comparison since the structures are different; while in the first reference a one-story prefabricated structure was the scope of study, in the second one a reinforced concrete story structure was the scope of research. In both, an increase in the structural period is evident. For the present work there are also increases in the period of the three scope structures (1-story, 2-story and 3-story SCH). (Table 4) presents the natural periods obtained, in each case.

**Table 4.** Natural periods of SCH with and without green roof

Green roof condition	1 Story (s)	2 Stories (s)	3 Stories (s)
No green roof	0.192	0.335	0.412
With green roof	0.228	0.387	0.490

## 10. Conclusions and future work

The conclusions of this work focus on two parts; the first part regarding the weight characterization of the green roof, and the second one regarding the structural impact of the implementation of this load on the structure of a SCH.

The mean weight of an extensive green roof in saturated condition with a 95% probability can be found between  $1.925 \text{ kN/m}^2$  and  $2.565 \text{ kN/m}^2$ . It is also clear that as the SCH gets higher, the structural vulnerability gets higher, with an increase in this condition by the green roof presence. For one-story structures, it is possible to implement a green roof in the northwestern part of the city. For structures with more than one story, it is not advisable because the structure, when subjected to an earthquake, can go from suffering moderate damage to severe damage and even reaching a stage close to collapse.

## 11. References

- A'saf, T. S.; Al-Ajlouni, M. G.; Ayad, J. Y.; Othman, Y. A.; St Hilaire, R. (2020). Performance of six different soilless green roof substrates for the Mediterranean region. *The Science of the Total Environment*, 730, 139182. <https://doi.org/10.1016/j.scitotenv.2020.139-182>
- Abhilash, R.; Biju, V.; Leslie, R. (2009). Effect of Lateral Load Patterns in Pushover Analysis. 10th National Conference on Technological Trends, November 2009.
- Aboelata, A. (2021). Assessment of green roof benefits on buildings' energy-saving by cooling outdoor spaces in different urban densities in arid cities. *Energy*, 219. <https://doi.org/10.1016/j.energy.2020.119514>
- Al-Chaar, G. K.; Lamb, G. E. (2002). Design of Fiber-Reinforced Polymer Materials for Seismic Rehabilitation of Infilled Concrete Structures. Final Report (Issue December, p. 83). <http://oai.dtic.mil/oai/oai?verb=getRecord&metadataPrefix=html&identifier=ADA411018>
- Apuntes. (2020). Techos verdes - Definición y beneficios por su aplicación - Selección de referentes. <http://apuntesdearquitecturadigital.blogspot.com/2020/03/techos-verdes-definicion-y-beneficios.html>
- Arroyo Amell, O. D.; Ramos Castillo, L. (2015). Necesidad de revisión de cargas y factores parciales de la NSR-10 para el diseño de estructuras sometidas a acciones de viento. *Ingeniería y Ciencia*, 11, 177–195. <https://doi.org/10.17230/ingciencia.11.21.9>
- Aşıkoğlu, A.; Vasconcelos, G.; Lourenço, P. B.; Pantò, B. (2020). Pushover analysis of unreinforced irregular masonry buildings: Lessons from different modeling approaches. *Engineering Structures*, 218. <https://doi.org/10.1016/j.engstruct.2020.110830>
- Bhandari, M. (2020). Prediction of inelastic response of base-isolated building frame by pushover analysis. *Asian Journal of Civil Engineering*, 21 (7), 1171–1182. <https://doi.org/10.1007/s42107-020-00267-7>
- Bianchini, F.; Rafiqul Haque, A. B. M.; Hewage, K.; Alam, M. S. (2016). Influence of green roofs on the seismic response of frame structures. *Earthquake and Structures*, 11(2), 265–280. <https://doi.org/10.12989/eas.2016.11.2.265>
- Cascone, S.; Catania, F.; Gagliano, A.; Sciuto, G. (2018). A comprehensive study on green roof performance for retrofitting existing buildings. *Building and Environment*, 136, 227–239. <https://doi.org/10.1016/j.buildenv.2018.03.052>
- Filippou, F.; Mazzoni, S. (2014). Concrete01 Material - Zero Tensile Strength. [https://opensees.berkeley.edu/wiki/index.php/Concrete01\\_Material\\_-\\_Zero\\_Tensile\\_Strength](https://opensees.berkeley.edu/wiki/index.php/Concrete01_Material_-_Zero_Tensile_Strength)
- Fundación Suiza de Cooperación para el Desarrollo Técnico. (2016). Situación actual de las viviendas de construcción de tipo informal en Villa el Salvador. <https://doi.org/10.1215/9780822387503-039>



ENGLISH VERSION.....

- Galambos, T. V.; Ellingwood, B.; MacGregor, J. G.; Cornell, C. A. (1982).** Probability based load criteria: assessment of current design practice. *ASCE Journal of Structural Division*. Vol. 108, Issue 5, Pg. 959-977
- IDIGER. (2020).** Caracterización General del Escenario de Riesgo Sísmico. <https://sire.gov.co/web/guest/rsismico>
- Khoshnoudian, F.; Mestri, S.; & Abedinik, F. (2011).** Proposal of lateral load pattern for pushover analysis of RC buildings. *Computational Methods in Civil Engineering*, 2(2), 169–183.
- López Borbón, W. (2018).** Diversidad informal urbana, intervenciones particulares para asentamientos específicos. Programas de mejoramiento barrial en Bogotá. *Bitácora Urbano Territorial*, 28(2), 135–142. Universidad Nacional de Colombia.
- López, W. (2016).** La informalidad urbana y los procesos de mejoramiento barrial. *Arquitectura y Urbanismo* vol. XXXVII, núm. 3, , pp. 1-18 <https://rau.cujae.edu.cu/index.php/revistaau/article/view/385>
- Mander, J. B; Priestley, M. J. N; Park, R. (1988).** Theoretical Stress Strain Model for Confined Concrete. *Journal of Structural Engineering*, Volume 114 Issue 8.
- Manso, M.; Teotónio, I.; Silva, C. M.; Cruz, C. O. (2021).** Green roof and green wall benefits and costs: A review of the quantitative evidence. *Renewable and Sustainable Energy Reviews*, 135 (August 2020). <https://doi.org/10.1016/j.rser.2020.110111>
- Marques, R.; Pereira, J. M.; Lourenço, P. B. (2020).** Lateral in-plane seismic response of confined masonry walls: From numerical to backbone models. *Engineering Structures*, 221 (July). <https://doi.org/10.1016/j.engstruct.2020.111098>
- Mohd Yassin, M. H. (1994).** Nonlinear Analysis of Prestressed Concrete Structures under Monotonic and Cycling Loads. University of California, Berkeley.
- Montgomery, D. C.; Runger, G. C. (2010).** Applied Statistics and Probability for Engineers (5th ed.). Wiley.
- Nektarios, P. A.; Kokkinou, I.; & Ntoulas, N. (2021).** The effects of substrate depth and irrigation regime, on seeded Sedum species grown on urban extensive green roof systems under semi-arid Mediterranean climatic conditions. *Journal of Environmental Management*, 279 (October 2020), 1–13. <https://doi.org/10.1016/j.jenvman.2020.111607>
- Nowak, A.; Collins, K. (1976).** Reliability of structures. McGraw Hill.
- Olaya, L.; Rubio, D.; Ruiz, D.; Torres, A. (2014).** Evaluación del comportamiento sísmico de viviendas de estratos marginales con cubiertas verdes: Estudio de caso del municipio de Soacha, Colombia. *Revista Ingeniería de Construcción*, 29 (1), 98–114. <https://doi.org/10.4067/s0718-50732014000100007>
- R, A. G.; S, H. K. (2000).** Estimation of seismic drift demands for frame structures. *Earthquake Engineering and Structural Dynamics*, 29 (March), 1287–1305.
- Rahmani, A. Y.; Bourahla, N.; Bento, R.; Badaoui, M. (2019).** Adaptive upper-bound pushover analysis for high-rise moment steel frames. *Structures*, 20 (January), 912–923. <https://doi.org/10.1016/j.istruc.2019.07.006>
- Rincón, A. F. (2010).** Vulnerabilidad sísmica de viviendas informales. Bogotá :Universidad de Los Andes.
- Sánchez de Guzmán, D. (2001).** Tecnología del concreto y el mortero (5th ed.). Editorial: Bhandar.
- Scott, M.; Filippou, F. (2016).** Hysteretic Material. [https://opensees.berkeley.edu/wiki/index.php/Hysteretic\\_Material](https://opensees.berkeley.edu/wiki/index.php/Hysteretic_Material)
- Sierra Guerrero, M. C.; Amarillo Suárez, Á. R. (2014).** Catálogo de la vegetación en jardines domésticos de Bogotá, Colombia. *Biota Colombiana*, 15(1), 10–46.
- Sun, J.; Tetsuro, O.; Zhao, Y.; Wang, W. (2003).** Lateral load pattern in pushover analysis. *Earthquake Engineering and Engineering Vibration*, 2(1), 99–107. <https://doi.org/10.1007/bf02857542>
- Valbuena Porras, S. G.; Mena Serna, M. (2011).** Caracterización del sistema constructivo y aspectos generales de la construcción de las viviendas populares en sectores vulnerables de la ciudad de Bogotá D.C. (p. 93).
- Welsh-Huggins, S. J.; Liel, A. B. (2017).** A life-cycle framework for integrating green building and hazard-resistant design: examining the seismic impacts of buildings with green roofs. *Structure and Infrastructure Engineering*, 13(1), 19–33. <https://doi.org/10.1080/15732479.2016.1198396>
- Zavala Toledo, C. (2019).** Damage Limit States for Confined Masonry Walls Based on Experimental Test. *Tecnia*, 29 (2), 135–141. <https://doi.org/10.21754/tecnia.v29i2.715>